

Fast sequential forensic camera identification

F. Pérez-González ^{#1}, I. González-Iglesias ^{#2}, M. Masciopinto ^{#3}, P. Comesaña ^{#4}

Signal Theory and Communications Department, University of Vigo

E. E. Telecomunicación, Campus-Lagoas Marcosende, Vigo 36310, Spain

{¹fperez, ²iglesias, ³mmasciopinto, ⁴pcomesan}@gts.uvigo.es

November 23, 2021

Abstract

Two sequential camera source identification methods are proposed. Sequential tests implement a log-likelihood ratio test in an incremental way, thus enabling a reliable decision with a minimal number of observations. One of our methods adapts Goljan et al.'s to sequential operation. The second, which offers better performance in terms of error probabilities and average number of test observations, is based on treating the alternative hypothesis as a doubly stochastic model. We also discuss how the standard sequential test can be corrected to account for the event of weak fingerprints. Finally, we validate the goodness of our methods with experiments.

1 Introduction

The PhotoResponse NonUniformity (PRNU) is a spatial pattern that acts as fingerprint or unique identifier of an image camera device. The PRNU is caused by minute imperfections in the image sensor manufacturing process, which remain constant over the life of the device. The PRNU is a variation in pixel responsivity and it arises when the device is illuminated [1]. Despite the PRNU is generally an extremely weak signal, given enough images samples and using signal processing techniques, it is possible to estimate it and use it as a robust fingerprint [2]. This fingerprint can be useful not only for source identification, but also for device linking, fingerprint matching, or forgery detection [3].

Nowadays, there are huge databases containing thousands of millions of images taken from many different cameras. To analyze whether any of those images was taken from a particular device, the computational cost would be enormous, since each processed image involves operations over more than 10^6 pixels for a typical image resolution.

The problem of fast source camera identification has been tackled in previous works [4, 5], always based on the idea of considering a so called *fingerprint digest* in-

stead of the whole fingerprint. However, to the best of our knowledge, there is no available PRNU detection method that works sequentially, i.e., that analyzes small blocks of pixels until enough reliability on the hypothesis test is achieved, thus guaranteeing that the minimum number of blocks is used to achieve a target accuracy. This is extremely valuable when checking very large amounts of images for the presence of a specific PRNU. Of particular interest to us is the fast source matching in huge databases used by the police to investigate child pornography and other cybercrime forensic cases. This is the topic of the European Project NIFTY [6] under which this work has been carried out.

In this paper, we revisit the PRNU estimation and detection problems, and propose a fast algorithm for source camera identification. Firstly, we derive a detector that improves the classical PRNU detection. Next, a sequential algorithm over pseudorandom subsets of pixels is proposed, performing the PRNU detection in a very fast way. Finally, the sequential versions of the detector in [7] and an improved detector are compared in terms of accuracy and average number of iterations of the sequential detector.

The paper is organized as follows: Sect. 2 reviews PRNU estimation and detection, drawing connections with existing methods, and proposing an improved detector. The fast sequential identification algorithm based on the improved detector is presented in Sect. 3. Sect. 4 shows experimental results on a dataset containing images from several devices, while Sect. 5 gives our conclusions.

Notation: Vectors are represented in boldface. The m th component of \mathbf{x} is denoted as x_m . The scalar product of vectors \mathbf{x} and \mathbf{y} is denoted by $\langle \mathbf{x}, \mathbf{y} \rangle$, while $\mathbf{x} \circ \mathbf{y}$ and $\|\mathbf{x}\|$ denote the sample-wise product and the Euclidean norm, respectively.

2 Model

We assume that the sensor output at pixel (i, j) , $y(i, j)$ can be written as [8]

$$y(i, j) = [1 + k(i, j)]x(i, j) + n(i, j), \quad (1)$$

where $k(i, j)$ is the (possibly gamma-corrected) PRNU and $n(i, j)$ subsumes a number of noise sources, including dark current, shot noise, read-out noise and quantization noise. As $x(i, j)$ is generally unknown, it is reasonable to obtain an estimate $\hat{x}(i, j)$ from $y(i, j)$ by applying some denoising procedure and accounting for demosaicing. In such case, we can write

$$y(i, j) = [1 + k(i, j)] \cdot [\hat{x}(i, j) + r(i, j)] + n(i, j), \quad (2)$$

where $r(i, j)$ is the denoising and demosaicing residue. For simplicity, we assume that $n(i, j) \sim \mathcal{N}(0, \sigma_n^2)$ and $r(i, j) \sim \mathcal{N}(0, \sigma_{i,j}^2)$, where the latter are mutually independent.

For compactness, we also introduce the *shifted PRNU*, which is 1+PRNU, i.e., $\kappa(i, j) \doteq [1 + k(i, j)]$.

2.1 PRNU estimation

From the model in (2), it is possible to formulate the PRNU estimation problem. We recall that in this case we have L available images taken with the same device from which we want to estimate the PRNU at every pixel. Assuming pixel-wise independence, we can solve the estimation problem independently for each pixel. Let then y_m and \hat{x}_m , $m = 1, \dots, L$, denote respectively the observation and the denoised image for an arbitrary pixel of the m th available image. Also let \mathbf{y} , $\hat{\mathbf{x}}$ be the vectors formed by stacking the L respective samples for the pixel under analysis. Then, the log-likelihood function becomes

$$L(\kappa, \hat{\mathbf{x}}, \mathbf{y}) = -\frac{1}{2} \left[\sum_{m=1}^L \log(2\pi\sigma_{e,m}^2) + \sum_{m=1}^L \frac{(\kappa\hat{x}_m - y_m)^2}{\sigma_{e,m}^2} \right], \quad (3)$$

where $\sigma_{e,m}^2 \doteq \kappa^2\sigma_m^2 + \sigma_n^2$, with σ_m^2 the variance of the estimation residue in image m (for the (i, j) th pixel, $\sigma_m^2 = \sigma_{i,j}^2$).

Taking the derivative of (3) with respect to κ and equating to zero, it is possible to write a (nonlinear) equation that gives the maximum likelihood estimate (MLE) of κ .

A simpler approach consists in neglecting the first term in (3). This gives a minimum weighted MSE solution, namely

$$\hat{\kappa} = \arg \min_{\kappa} \sum_{m=1}^L \frac{(\kappa\hat{x}_m - y_m)^2}{\sigma_{e,m}^2}. \quad (4)$$

When $\sigma_m^2 = \sigma_r^2$ for all $m = 1, \dots, L$, then taking the derivative with respect to κ and setting to zero, we obtain that $\hat{\kappa}$ must be a solution to the equation

$$\hat{\kappa}^2 \langle \hat{\mathbf{x}}, \mathbf{y} \rangle \sigma_r^2 + (||\hat{\mathbf{x}}||^2 \sigma_n^2 - ||\mathbf{y}'||^2 \sigma_r^2) \hat{\kappa} - \langle \hat{\mathbf{x}}, \mathbf{y} \rangle \sigma_n^2 = 0. \quad (5)$$

Assuming that $\sigma_n^2 \gg \sigma_r^2$, the solution to (5) becomes $\hat{\kappa} = \langle \hat{\mathbf{x}}, \mathbf{y} \rangle / ||\hat{\mathbf{x}}||^2$ or equivalently, in terms of the PRNU \hat{k} ,

$$\hat{k} = \frac{\langle (\mathbf{y} - \hat{\mathbf{x}}), \hat{\mathbf{x}} \rangle}{||\hat{\mathbf{x}}||^2}, \quad (6)$$

which in fact resembles Chen et al.'s estimator $\hat{k} = \langle (\mathbf{y} - \hat{\mathbf{x}}), \mathbf{y} \rangle / ||\mathbf{y}'||^2$ in [8], as $\hat{\mathbf{x}} \approx \mathbf{y}$.

2.2 PRNU detection

Once a PRNU estimate is available, it can be used for camera identification purposes. This is in fact a detection problem that can be cast as follows. Given a set of L images which have been taken from the same camera with PRNU \mathbf{k}_0 , and a test image \mathbf{y}_t , both arranged in vector form, we want to decide whether \mathbf{y}_t has been taken from that camera or, in other words, if the PRNU \mathbf{k}_0 is present in \mathbf{y}_t . As customary, we can formulate a binary hypothesis test with the following two hypotheses:

- H_0 : Image \mathbf{y}_t does not contain the PRNU \mathbf{k}_0 ,
- H_1 : Image \mathbf{y}_t contains the PRNU \mathbf{k}_0 .

We assume the existence of an unbiased estimate $\hat{\mathbf{k}}$ of \mathbf{k}_0 obtained using the method proposed in the previous section, and we denote by $\hat{\mathbf{x}}_t$ the image vector obtained from \mathbf{y}_t after denoising and demosaicing. We have derived the corresponding distributions under each hypothesis; this allows us to write Neyman-Pearson's generic detector for known \mathbf{k}_0 , and later replace the needed statistics by their estimates, as in the *Generalized Likelihood Ratio Test* (GLRT).

Thus, when H_1 holds, we can see that the difference $y_t(i, j) - \hat{x}_t(i, j)$ for the (i, j) th pixel is Gaussian with mean $k_0(i, j) \cdot \hat{x}_t(i, j)$ and variance

$$\sigma_H^2 = [1 + k_0(i, j)]^2 \sigma_r^2 + \sigma_n^2 \approx \sigma_r^2 + \sigma_n^2. \quad (7)$$

When H_0 holds, the PRNU must be treated as unknown. Modeling it as a zero-mean random variable, it follows that $y_t(i, j) - \hat{x}_t(i, j)$ is approximately Gaussian with zero mean and variance approximately σ_H^2 , because the influence of the variance of the PRNU in the total variance is negligible. From this, the likelihood-ratio test can be written as

$$\frac{\langle (\mathbf{y}_t - \hat{\mathbf{x}}_t), \mathbf{k}_0 \circ \hat{\mathbf{x}}_t \rangle}{\sigma_H^2} - \frac{\|\mathbf{k}_0 \circ \hat{\mathbf{x}}_t\|^2}{2\sigma_H^2} \underset{H_0}{\overset{H_1}{\gtrless}} \eta \quad (8)$$

for some threshold η that is chosen so as to produce the desired probability of false positive.

The implementation (8) faces two practical problems: 1) The true PRNU \mathbf{k}_0 is unknown; 2) σ_H^2 is unknown. To overcome the first problem, one may think of substituting $\langle (\mathbf{y}_t - \hat{\mathbf{x}}_t), \mathbf{k}_0 \circ \hat{\mathbf{x}}_t \rangle$ by $\langle (\mathbf{y}_t - \hat{\mathbf{x}}_t), \hat{\mathbf{k}} \circ \hat{\mathbf{x}}_t \rangle$ after noticing that

$$\langle (\mathbf{y}_t - \hat{\mathbf{x}}_t), \mathbf{k}_0 \circ \hat{\mathbf{x}}_t \rangle = E \left\{ \langle (\mathbf{y}_t - \hat{\mathbf{x}}_t), \hat{\mathbf{k}} \circ \hat{\mathbf{x}}_t \rangle \right\}. \quad (9)$$

However, the results obtained by following this approach are rather disappointing in practice because the variance of the estimation error in $\hat{\mathbf{k}}$ significantly affects the computation of the second summand in (8).

Focusing on the first term of (8) produces one (generally, non-sufficient) statistic that is very similar to which has been proposed by Goljan *et al.* [7]:¹

$$u \doteq \langle (\mathbf{y}_t - \hat{\mathbf{x}}_t), \hat{\mathbf{k}} \circ \hat{\mathbf{x}}_t \rangle, \quad (10)$$

and, as we argue above, the means for the respective hypotheses are

$$E\{u|H_0\} = 0; \quad E\{u|H_1\} = E\{\|\mathbf{k}_0 \circ \mathbf{x}_t\|^2\}. \quad (11)$$

Let us define the shift operator $\Delta_{(q_1, q_2)}$ that applied to a vector \mathbf{x} representing an image, outputs the vector corresponding to a right circular shift of (q_1, q_2) pixels

¹Goljan *et al.* use \mathbf{y}_t instead of $\hat{\mathbf{x}}_t$ in the second term of the scalar product.

of such image. Then, following [7], an estimate of the variance of statistic u can be obtained as,

$$\hat{\sigma}_u^2 = \frac{1}{M - |A|} \sum_{(q_1, q_2) \notin A} \langle \Delta_{(q_1, q_2)}(\mathbf{y}_t - \hat{\mathbf{x}}_t), \hat{\mathbf{k}} \circ \hat{\mathbf{x}}_t \rangle^2, \quad (12)$$

where M is the number of available pixels, A is an *exclusion set* defined as those (q_1, q_2) in a neighborhood (w. r. t. circular shifts) of the origin $(0, 0)$, and $|A|$ denotes its cardinality.

Since $E\{u|H_1\}$ is difficult to obtain accurately, it may be reasonable to assume that under H_1 the statistic u has a positive but unknown mean. Then, from Karlin-Rubin theorem [9], the test

$$u' \underset{H_0}{\overset{H_1}{\gtrless}} \eta_2, \quad (13)$$

where $u' \doteq u/\hat{\sigma}_u$, is the uniformly most powerful test for a given probability of false positive P_F . However, notice that even though the test threshold η_2 can be set since P_F is computable, we cannot find the detection probability P_D as the mean under H_1 is unknown. This has important implications for the tests discussed in Sect. 3. Obviously, better performance would be expected if $\mu_{u,1} \doteq E\{u'|H_1\}$ were known.

2.3 Improved detector

Although $\mu_{u,1}$ is not known, we have found that it can be modeled as a normal random variable whose parameters depend on the statistic

$$v \doteq \|\hat{\mathbf{k}} \circ \hat{\mathbf{x}}_t\|^2 / \hat{\sigma}_u, \quad (14)$$

so we will denote by $\mu(v)$ and $\sigma^2(v)$ the mean and variance of $\mu_{u,1}$, respectively. Thus, $\mu_{u,1} \sim \mathcal{N}(\mu(v), \sigma^2(v))$. Notice that the statistic v resembles the second term in (8) but obtained from computable quantities. However, the laws $\mu(v)$ and $\sigma^2(v)$ are device-dependent, so they must be learned during the PRNU extraction phase, which can be done concurrently with the estimation of \mathbf{k}_0 . Furthermore, although the distribution of u' under H_0 can be modeled by a Gaussian, a slight improvement is afforded by employing a zero-mean generalized Gaussian distribution with scale parameter α_0 and shape parameter c_0 , which can be reliably estimated using images from different cameras [10] (see Sect. 2.4).

With all these considerations, the test becomes

$$\left(\frac{|u'|}{\alpha_0} \right)^{c_0} - \frac{(u' - \mu(v))^2}{2\sigma^2(v)} \underset{H_0}{\overset{H_1}{\gtrless}} \eta_3. \quad (15)$$

2.4 Model training

At this point, it is necessary to estimate the model parameters for both hypotheses. For H_1 , $\mu(v)$ and $\sigma^2(v)$ must be estimated for the target camera, while for H_0 the parameters α_0 and c_0 are estimated from the universe of available images.

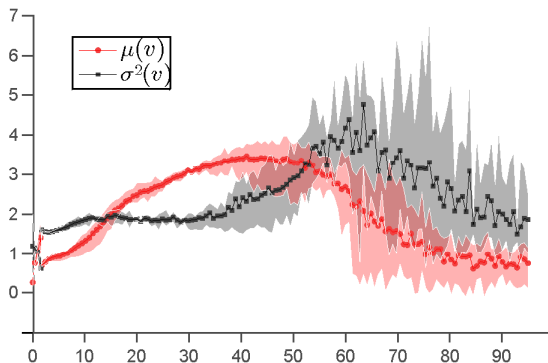


Figure 1: Parameters $\mu(v)$ and $\sigma^2(v)$ learned from $L = 50$ images during the training phase for camera Nikon D60.

As mentioned, the estimation of the mean and variance of $\mu_{u,1}$ is done concurrently with the estimation of $\hat{\mathbf{k}}$. Let \mathbf{y}_{tr} be one of the L available images for training. Then, $\hat{\mathbf{k}}$ is estimated from the remaining $L - 1$ images, and pairs of (u', v) values are obtained from \mathbf{y}_{tr} and $\hat{\mathbf{k}}$ by taking subsets of pixels with the same size as that used in the hypothesis test. This process is repeated for each of the L images in the training set to produce a collection of (u', v) pairs that is used to estimate $\mu(v)$ and $\sigma^2(v)$. This is done by binning the values of v and for each bin calculating the mean and variance of the corresponding set of u' values.

For illustration purposes, Fig. 1 shows an example of the laws $\mu(v)$ and $\sigma^2(v)$ obtained by applying the explained procedure. The color bands represent the range of values for 5 different trainings (each training with $L = 50$ randomly selected images) over the same device.

When the subsets of pixels used for training do not have the same size as for the hypothesis test, the scaling factor $\sqrt{M_t/M_{tr}}$ must be applied on v , $\mu(v)$ and $\sigma^2(v)$, where M_{tr} and M_t stand for the number of available training and testing pixels, respectively. We note, however, that if the sizes are significantly different, the correction may yield unsatisfactory results.

3 Sequential test for fast PRNU detection

The Sequential Probability Ratio Test (SPRT) was proposed by A. Wald in [11]. On a hypothesis testing problem, the main purpose of the SPRT is minimize the expected number of observations to achieve error probabilities less than a pre-fixed target probabilities of misdetection (P_M^*) and false positive (P_F^*).

Let x_1, x_2, \dots, x_n be i.i.d. observations, with n its number, and $f(x_j|H_i)$ the probability density function (pdf) of the j th observation conditioned on the i th hypothesis

($i = 0, 1$). In a SPRT the likelihood ratio is compared with two thresholds. If

$$B < \prod_{j=1}^n \frac{f(x_j|H_1)}{f(x_j|H_0)} < A, \quad (16)$$

the test continues and another observation (a.o.) is taken. If

$$\prod_{j=1}^n \frac{f(x_j|H_1)}{f(x_j|H_0)} \geq A, \quad (17)$$

the test accepts the alternative hypothesis (H_1). If

$$\prod_{j=1}^n \frac{f(x_j|H_1)}{f(x_j|H_0)} \leq B, \quad (18)$$

the test accepts the null hypothesis (H_0).

The thresholds are chosen so as to control the error probabilities on each hypothesis. Following Wald's approximation [11], the relations between the maximum permissible errors (P_M^* and P_F^*) and the thresholds are

$$A \leq \frac{1 - P_M^*}{P_F^*}, \quad B \geq \frac{P_M^*}{1 - P_F^*}, \quad (19)$$

where the equality is usually a good choice in practice.

Therefore, the hypothesis testing problem discussed in Sect. 2.2 and, hence, our proposed detector in (15), can be transformed into a SPRT by taking logarithms in (16-18). Then, the resulting SPRT is

$$\eta_B \underset{\text{a.o.}}{\gtrsim} \sum_{j=1}^n D_j \underset{\text{a.o.}}{\gtrsim} \eta_A, \quad (20)$$

where the thresholds are $\eta_A = \log(A) - n \cdot \log(2\alpha_0\Gamma(1/c_0))$ and $\eta_B = \log(B) - n \cdot \log(2\alpha_0\Gamma(1/c_0))$, and

$$D_j \doteq \left(\frac{|u'_j|}{\alpha_0} \right)^{c_0} - \frac{(u'_j - \mu(v_j))^2}{2\sigma^2(v_j)} - \log \left(c_0 \sqrt{2\pi\sigma^2(v_j)} \right). \quad (21)$$

Figure 2 summarizes the proposed algorithm for fast source camera identification. Given a test image y_t , the pixels are pseudorandomly assigned to subsets \mathcal{S}_j , $j = 1, \dots, n$, with T pixels each. The j th observation (u'_j, v_j) is computed by using in (10) and (14) only those pixels in subset \mathcal{S}_j . A maximum number of observations N is set for the SPRT; if n reaches that value without a decision being taken, the entire image is analyzed with a non-sequential test. In addition, those images classified as H_1 by the SPRT are retested using the whole image, in order to achieve the minimum possible error probabilities.

In setting the thresholds A and B , we notice that we aim at achieving a very small probability of misdetection P_M , whereas we do not care as much about P_F , because the subsequent full-image test will discard most false positives.

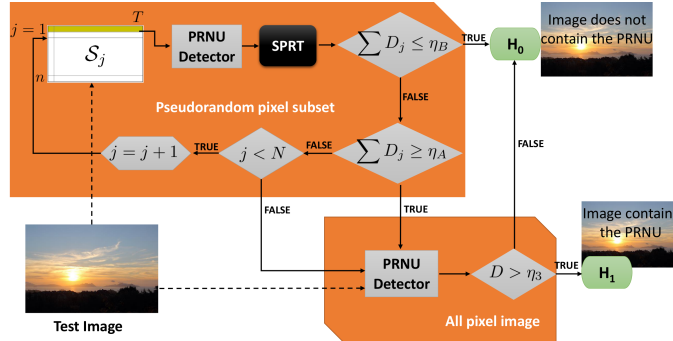


Figure 2: Sequential test implementation.

3.1 Fixed-parameter PRNU Sequential Test

Here we propose a SPRT based on the well-known detection method by Goljan et al. in [7]. Such method sets the detection threshold on the basis of a target P_F , but entirely disregards hypothesis H_1 and, consequently, P_M . See (13). However, knowledge of P_M is necessary to implement a SPRT as is apparent from (19).

In contrast, our detector in (15) derived in Sect. 2.3 overcomes this issue, as now the distribution of u' under H_1 is well defined. On the other hand, as we noticed in Sect. 2.4, in some cases a deficient training phase may lead to bad estimates of $\mu(v)$ and $\sigma^2(v)$, which would have a large impact on the detection performance. To propose a feasible solution to those cases and at the same time quantify how much is gained by learning $\mu(v)$ and $\sigma^2(v)$, we have also studied the performance of our detector in (15) when $\mu(v)$ and $\sigma^2(v)$ are assumed to be independent of v . The results are reported in Sect. 4.

3.2 Dealing with weak PRNUs

Although the model used in Sect. 2.3 fits quite well the statistical distributions for both hypotheses, there are cases where the PRNU is weak due to the contents of the image [8]. As discussed in Sect. 2.4, the mean $\mu(v_j)$ may vary significantly among different observed subsets S_j . For very dark images $v \approx 0$ and $\mu(v)$ may be very close to zero, implying that both hypotheses are barely distinguishable. Another problematic case occurs when an image presents many white or saturated pixels at any color channel, since saturated pixels are PRNU-free. Despite the model fits quite well u' under hypothesis H_1 , we have noticed experimentally that some images contain most of the observations u'_j on the left tail of H_1 , to the point that those images are wrongly classified as H_0 after the SPRT has processed a few initial observations. See Fig. 3 for an illustration of the overlap between the left tails of H_0 and H_1 , with also their matching pdf's for fixed parameters, i.e., independent of v .

In order to address those outliers, we introduce a probability $p \in [0, 1)$ that the observations $u'_j|H_1$ follow the distribution corresponding to H_0 (i.e., the probability that the observations for H_1 do not contain the PRNU). We next show that when $p > 0$

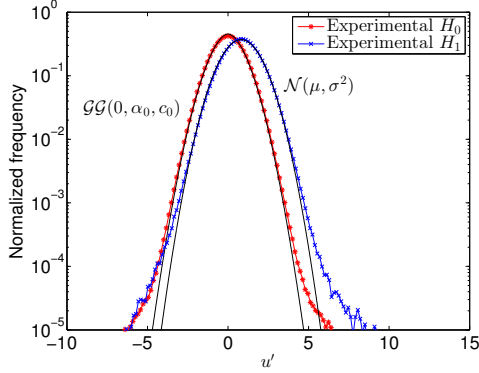


Figure 3: Log-plot of experimental and theoretical distributions of u' under both hypotheses for 1024 random pixels. Camera Nikon D60 is used for the hypothesis H_1 , resulting on $\mu = 0.81$ and $\sigma^2 = 1.17$. The parameters for H_0 are $\alpha_0 = 1.24$ and $c_0 = 1.78$.

the SPRT requires that the thresholds A and B be modified as P_M will change (P_F does not, as H_0 remains the same). If P'_M denotes the new misdetection probability, it is easy to show that $P'_M = p \cdot (1 - P_F) + (1 - p) \cdot P_M$.

Therefore, to achieve a certain target misdetection probability P'^*_M , the thresholds must be recomputed by substituting

$$P^*_M = \frac{P'^*_M - p \cdot (1 - P_F)}{1 - p} \quad (22)$$

into the expressions in (19). An important remark is that the presence of outliers imposes a bound on the achievable detection probability $P^*_D = (1 - P^*_M)$, namely, $P^*_D \leq 1 - p \cdot (1 - P_F)$.

Thus, in practice, the maximum achievable P_D may be below the target. If such is the case, then it is necessary to give up on the target P_F , i.e., a larger value will be achieved. This has a limited impact in practice because we remind that all the positives from the SPRT are later subject to a full-image test which will discard most of those false positives. The increase of P_D can be achieved by multiplying both A and B by a factor $\beta \leq 1$.

3.3 Fast variance estimation

The variance estimator $\hat{\sigma}_u^2$ in (12) is taken from [7], which is quite time-consuming as it contains two nested sums (corresponding to the scalar product and the averaging over the spatial shifts). Since one of the aims of the methods proposed in this paper is to reduce the detection time, we propose the following simpler estimator

$$\hat{\sigma}'_u{}^2 = \frac{1}{M} \|\hat{\mathbf{k}} \circ \hat{\mathbf{x}}_t\|^2 \|(\mathbf{y}_t - \hat{\mathbf{x}}_t)\|^2. \quad (23)$$

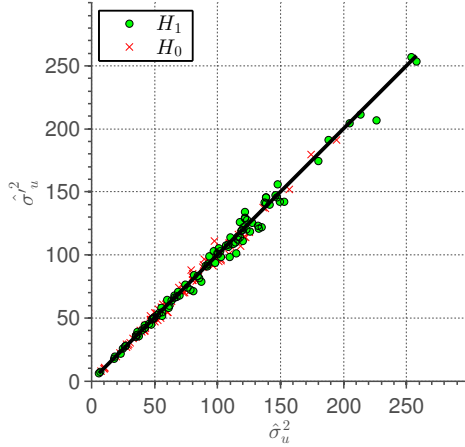


Figure 4: Values of $\hat{\sigma}_u^2$ versus $\hat{\sigma}'_u^2$ for 100 samples from each hypothesis. Each sample is from a 32×32 block-size for 147 images taken with Nikon D60.

Figure 4 shows that there is a very little difference between $\hat{\sigma}_u^2$ and $\hat{\sigma}'_u^2$ under both hypotheses. In fact, in terms of camera identification performance, there is no significant difference between both variance estimation methods, since the Areas Under Curve (AUCs) for the respective Receiver Operating Characteristic (ROC) curves are practically identical (differences show up in the 4th significant digit).

In terms of computing time, if M is the total number of pixels in the image and $|A|$ is the size of the exclusion set, the estimator in (23) is $M - |A| \approx M$ times faster, which even for small-sized images results in enormous savings.

4 Experimental results

The image database for the experimental results is a collection of pictures from different sources. The database is composed of TIFF images coming from our own cameras, the Dresden image database [12], and the Raise database [13]. Some camera models include more than one device as Table 1 shows. The table specifies the number of images from each device as well as some camera model characteristics.

For PRNU extraction, $L = 50$ images are randomly selected for those devices in Table 1 with more than 50 images available. The PRNU is extracted as described in Sect. 2.1. The experimental results sequentially pick as hypothesis H_1 each device with more than 50 images, and H_0 all the database images from the remaining devices in Table 1.

In order to make the results independent of the specific choice of L images and also to increase the number of test images corresponding to H_1 , the reported results are the average of 5 different random selections of the L images, using the remaining images of each selection to test H_1 .

In all the experiments, the denoised images $\hat{\mathbf{x}}_t$ are obtained using the same filter as

Table 1: Cameras used in SPRT experiments with characteristics, number of devices for each model, number of images for each device and database source.

Camera Model	Sensor	Native resolution	Devices	Number of images	Database
Canon 600D	22.3x14.9mm CMOS	5184x3456	1	241	Own
Canon 1100D	23.2x14.7mm CMOS	4272x2848	3	316/122/216	Own
Nikon D60	23.6x15.8mm CCD	3872x2592	1	197	Own
Nikon D70	23.7x15.6mm CCD	3008x2000	2	43/43	Dresden
Nikon D70S	23.7x15.6mm CCD	3008x2000	2	43/47	Dresden
Nikon D90	23.6x15.8mm CMOS	4288x2848	1	250	Raise
Nikon D200	23.6x15.8mm CCD	3872x2592	2	48/43	Dresden
Nikon D3000	23.6x15.8mm CCD	3872x2592	1	230	Own
Nikon D3200	23.2x15.4mm CMOS	6016x4000	1	250	Own
Nikon D5100	23.6x15.6mm CMOS	4928x3264	1	250	Own
Nikon D7000	23.6x15.6mm CMOS	4928x3264	1	250	Raise

in [8]. In addition, the estimated PRNU in (6) is postprocessed to remove the unwanted artifacts discussed in [8]; this postprocessing includes mean-subtraction and Wiener filtering in the Fourier domain.

For each test image \mathbf{y}_t , pseudorandom non-overlapping subsets \mathcal{S}_j of size 1024 pixels, $j = 1, \dots, N$, are taken. The maximum number of observations N is fixed to 256 because we have experimentally found that for TIFF images a size of 512×512 should be enough for successful PRNU detection. The results obtained after the SPRT described in Sect. 3 are shown in Table 2, where \bar{n}_{H_0} and \bar{n}_{H_1} denote the average number of observations that the SPRT needs in order to make a decision for H_0 and H_1 , respectively. The parameters for the hypothesis H_0 were set to $\alpha_0 = 1.24$ and $c_0 = 1.78$ after applying the maximum likelihood estimation criterion. These parameters remain fixed throughout all the experiments. Figure 5 shows the SPRT observation track of some classified and misclassified images.

As seen in Table 2, for several cameras the empirical values of P_D do not meet the target of 0.98. For this reason, we have applied the correction methods discussed in Sect. 3.2, obtaining the results reported in Table 3.

An important analysis over the proposed SPRT is to measure the computational savings achieved with respect to a full-image test. Given O_F as the computational cost of classifying a full image, and O_S the computational cost under our SPRT detector, both are directly proportional to the respective number of pixels. The total number of pixels is M , where as for the SPRT detector is $M' = \bar{n}T$, where \bar{n} is the average number of observations which can be written as

$$\bar{n} = \bar{n}_0 \cdot p_{H_0} + \bar{n}_1 \cdot p_{H_1}, \quad (24)$$

with \bar{n}_0, \bar{n}_1 the average of $\bar{n}_{H_0}, \bar{n}_{H_1}$ over all devices in Table 3, and $p_{H_0}, p_{H_1} = (1 - p_{H_0})$ the prior probabilities of hypotheses H_0, H_1 , respectively.

On the other hand, when testing a large database with the SPRT, the computational

Table 2: Experimental results for both SPRTs. $P_D^* = 0.98$ and $P_F^* = 0.3$.

Device	Proposed SPRT				SPRT with fixed μ and σ^2			
	P_D	\bar{n}_{H_1}	P_F	\bar{n}_{H_0}	P_D	\bar{n}_{H_1}	P_F	\bar{n}_{H_0}
Canon 600D	0.9895	1.07	0.0083	1.73	0.9895	1.08	0.0078	1.75
Canon 1100D #1	0.9398	2.61	0.0933	4.24	0.9323	2.50	0.0897	3.97
Canon 1100D #2	0.9028	6.24	0.1449	10.04	0.8750	6.53	0.1439	10.17
Canon 1100D #3	0.9880	3.98	0.1451	9.04	0.9940	4.02	0.1450	9.25
Nikon D60	0.9660	6.11	0.1869	8.65	0.9456	5.84	0.1874	9.50
Nikon D90	0.8800	5.18	0.1870	10.94	0.8800	5.50	0.1797	10.72
Nikon D3000	0.9778	2.59	0.1338	4.64	0.9722	2.67	0.1336	4.63
Nikon D3200	0.9900	2.63	0.1276	4.60	0.9850	2.51	0.1298	4.58
Nikon D5100	0.9750	7.86	0.2095	12.51	0.9800	8.45	0.2162	17.57
Nikon D7000	0.9350	5.45	0.2106	10.45	0.9200	5.42	0.2021	9.27

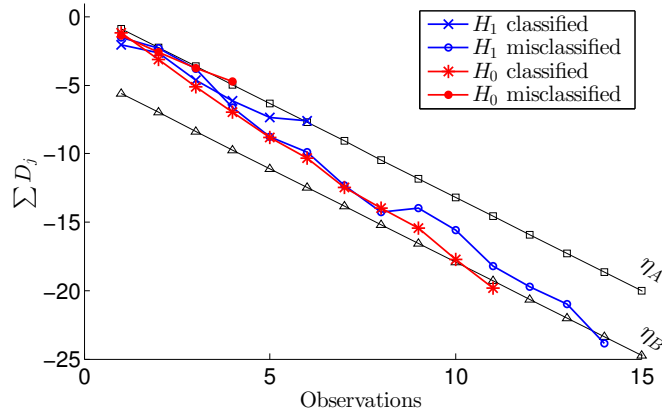


Figure 5: SPRT observations track.

cost is proportional to $O_S + [P_D^* p_{H_1} + P_F^* p_{H_0}] \cdot O_F$, where term in brackets is the probability that the test gives a (true or false) positive. Then, the saving is given by the following ratio

$$\frac{O_S}{O_F} = P_D^* \cdot p_{H_1} + P_F^* \cdot p_{H_0} + \bar{n}T/M. \quad (25)$$

For a database with images of size $M = 2000 \times 3000$ pixels and $p_{H_1} = 0.01$, a sequential detector with subsets of size $T = 1024$, and the P_D^*, P_F^* values of Table 3, the ratio in (25) is approximately 0.3. Furthermore, the computation of the estimated variance following the simplification in Sect. 3.3 would produce an additional huge reduction of $1/M \approx 1.6 \cdot 10^{-7}$.

Finally, in order to compare the proposed detector in Sect. 2.3 (I-SPRT) and its version with fixed μ and σ^2 (F-SPRT), we averaged over the cameras the respective detection probabilities in Table 3 as well as the average number of observations \bar{n} .

Table 3: Experimental results for both SPRTs. $P_D^* = 0.98$, $P_F^* = 0.3$, $p = 0.0285$, $\beta = 0.65$.

Device	Proposed SPRT				SPRT with fixed μ and σ^2			
	P_D	\bar{n}_{H_1}	P_F	\bar{n}_{H_0}	P_D	\bar{n}_{H_1}	P_F	\bar{n}_{H_0}
Canon 600D	1.0000	1.14	0.0120	3.85	1.0000	1.14	0.0117	3.92
Canon 1100D #1	0.9737	3.31	0.1389	10.08	0.9774	3.30	0.1327	9.43
Canon 1100D #2	0.9861	6.35	0.2242	24.70	0.9722	6.58	0.2227	25.25
Canon 1100D #3	1.0000	3.44	0.2225	22.24	1.0000	3.41	0.2223	22.80
Nikon D60	0.9864	6.12	0.2715	21.12	0.9728	5.67	0.2740	23.39
Nikon D90	0.9400	8.00	0.2760	26.81	0.9300	8.69	0.2658	26.78
Nikon D3000	0.9944	2.30	0.1916	11.13	0.9944	2.32	0.1891	11.16
Nikon D3200	1.0000	2.35	0.1796	11.10	1.0000	2.32	0.1813	11.04
Nikon D5100	0.9900	7.38	0.3039	30.10	0.9900	7.14	0.3168	44.10
Nikon D7000	0.9900	6.48	0.3067	25.46	0.9700	6.94	0.2923	22.55

Notice that we do not compare here on the basis of P_F , since the images wrongly classified as H_1 will be analyzed a second time (see Fig. 2). We obtained the following results: $\bar{P}_D^I = 0.986$, $\bar{P}_D^F = 0.981$, $\bar{n}^I = 18.5$ and $\bar{n}^F = 19.9$, where the superscripts I and F denote I-SPRT and F-SPRT, respectively. As we can see, the improved detector offers a small gain in both indicators, so its use is advised despite the extra computation required in the training phase.

5 Conclusions

In this paper we have shown how Wald's sequential test can be implemented for PRNU detection purposes, with the advantage of enabling a very fast test that makes a reliable decision with a minimum number of observations. The test is corrected to account for the event that under H_1 the observations may contain very weak fingerprints. The proposed tests are especially useful when very large databases must be searched for device identification.

Acknowledgments

Research supported by the Illegal use of Internet (INT) call within the Prevention of and Fight against Crime (ISEC) programme of the Home Affairs Department of the European Commission under project NIFTY (Project Number HOME/2012/ISEC/AG/INT/4000003892), the European Regional Development Fund (ERDF) and the Galician Regional Government under agreement for funding the Atlantic Research Center for Information and Communication Technologies (AtlantTIC), the Spanish Government and the European Regional Development Fund (ERDF) under project TACTICA, the European Regional Development Fund (ERDF) and the Spanish Government under project COMONSENS (CONSOLIDER-INGENIO 2010 CSD2008-00010), and the Galician Regional Government under projects "Consolidation of Research Units" 2009/62, 2010/85.

References

- [1] G. C. Holst, *CCD Arrays, Cameras, and Displays*, 2nd ed. SPIE Optical Engineering Press Bellingham, WA, 1998.

- [2] J. Lukáš, J. Fridrich, and M. Goljan, "Digital camera identification from sensor pattern noise," *IEEE Trans. Inf. Forensics Security*, vol. 1, no. 2, pp. 205–214, Jun. 2006.
- [3] J. Fridrich, "Digital image forensics," *IEEE Signal Process. Mag.*, vol. 26, no. 2, pp. 26–37, Mar. 2009.
- [4] M. Goljan and J. Fridrich, "Sensor fingerprint digests for fast camera identification from geometrically distorted images," in *Proc. SPIE*, vol. 8665, Mar. 2013, pp. 86 650B-1–86 650B-10.
- [5] Y. Hu, C.-T. Li, Z. Lai, and S. Zhang, "Fast camera fingerprint search algorithm for source camera identification," in *Proc. 5th Int. Symp. Commun. Control Signal Process. (ISCCSP)*, May 2012, pp. 1–5.
- [6] NIFTY website. [Online]. Available: <http://research.ncl.ac.uk/nifty/>
- [7] M. Goljan, J. Fridrich, and T. Filler, "Large scale test of sensor fingerprint camera identification," in *Proc. SPIE*, vol. 7254, Feb. 2009, pp. 72 540I-1–72 540I-12.
- [8] M. Chen, J. Fridrich, M. Goljan, and J. Lukáš, "Determining image origin and integrity using sensor noise," *IEEE Trans. Inf. Forensics Security*, vol. 3, no. 1, pp. 74–90, Mar. 2008.
- [9] S. Karlin and H. Rubin, "The theory of decision procedures for distributions with monotone likelihood ratio," *The Annals of Mathematical Statistics*, vol. 27, no. 2, pp. 272–299, Jun. 1956.
- [10] K. Birney and T. Fischer, "On the modeling of DCT and subband image data for compression," *IEEE Trans. Signal Process.*, vol. 4, no. 2, pp. 186–193, Feb. 1995.
- [11] A. Wald, "Sequential tests of statistical hypotheses," *The Annals of Mathematical Statistics*, vol. 16, no. 2, pp. 117–186, Jun. 1945.
- [12] T. Gloe and R. Böhme, "The 'Dresden Image Database' for benchmarking digital image forensics," in *Proc. of the 25th Symp. On Applied Computing (ACM SAC 2010)*, vol. 2, Mar. 2010, pp. 1585–1591.
- [13] D.T. Dang-Nguyen, C. Pasquini, V. Conotter and G. Boato, "Raise a raw images dataset for digital image forensics," in *Proc. 6th ACM Multimedia Systems Conference*. ACM, Mar. 2015, pp. 219–224.